# Extreme Ultraviolet Light Shaping and Spectroscopy through Opto-Optical Modulation

Olofsson, Anna

2021

*Document Version:*
Publisher's PDF, also known as Version of record

# Extreme Ultraviolet Light Shaping and Spectroscopy through Opto-Optical Modulation

ANNA OLOFSSON
FACULTY OF ENGINEERING | LUND UNIVERSITY

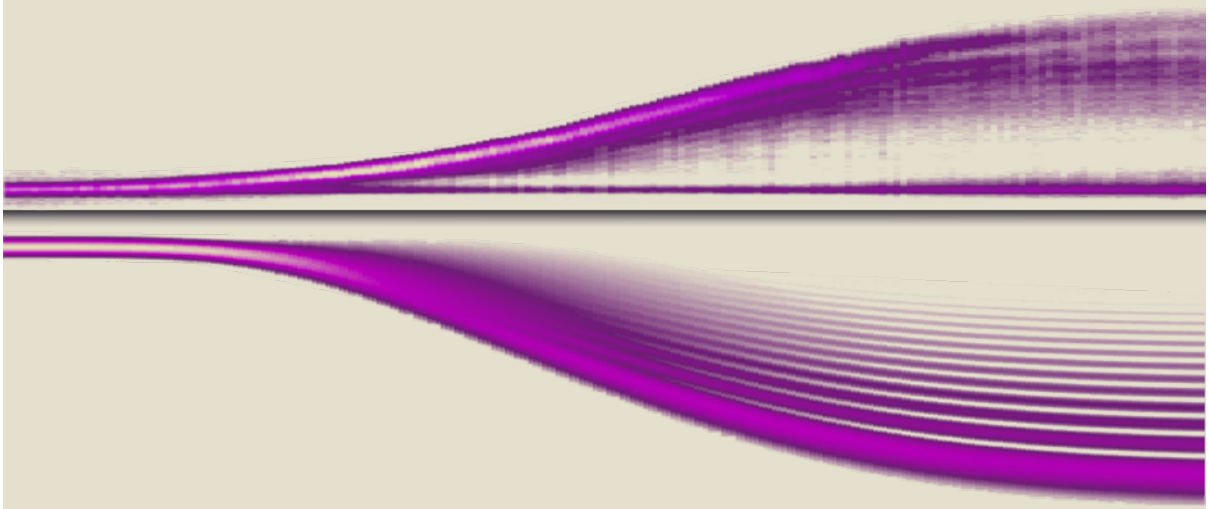

# Extreme Ultraviolet Light Shaping and Spectroscopy through Opto-Optical Modulation

# Extreme Ultraviolet Light Shaping and Spectroscopy through Opto-Optical Modulation

by Anna Olofsson


LUND
UNIVERSITY

Thesis for the degree of Licentiate
Thesis advisors: Prof. Johan Mauritsson, Dr. Emma R. Simpson, Prof. Anne l'Huillier and Dr. Lars Rippe
Faculty opponent: Morten Bache

To be presented, with the permission of the Faculty of Science of Lund University, for public criticism in room 404 at the Department of Physics, on Friday the 29th of October 2021 at 13.15.

| Organization | Document name |
|---|---|
| **LUND UNIVERSITY**<br>Department of Physics<br>Box 124<br>SE–221 00 LUND<br>Sweden | **LICENTIATE THESIS**<br>Date of disputation<br>2021-10-29<br>Sponsoring organization |
| Author(s)<br>Anna Olofsson | |


Title and subtitle

Extreme Ultraviolet Light Shaping and Spectroscopy through Opto-Optical Modulation


Abstract

Extreme ultraviolet (XUV) light is a central component in many methods to study the world around us. The research fields that use XUV light span many different topics; XUV light is for example a key component when the world's shortest (at the time of writing) light pulses are produced. XUV light is typically resonant with atomic transitions from the ground state to high energy levels or ionization of an inner shell electron, which makes it a very useful tool for spectroscopy. However, this property also makes it problematic to work with XUV beams, as typical optical tools based on transmission will have their intrinsic material changed by the passage of the XUV light. It is therefore interesting to develop new control techniques for light in the XUV. In this thesis I present how XUV light can be controlled by using an atomic ensemble as control medium. An XUV pulse excites the atomic ensemble, which starts to re-radiate XUV light. The control of this emission is exerted through control of the emission wavefront. This is achieved by a second light pulse (infrared for the research this thesis is based on), that induces a Stark shift of the energy levels of the atomic ensemble. The Stark shift is intensity-dependent, thus, control of the intensity profile of the second pulse gives control of the phase modulation of the XUV emission from the atomic ensemble. This thesis is concerned partly with the possibility to shape the XUV light, also in a non-linear fashion, by controlling the intensity profile of the second pulse. However, this thesis also delves into the possibility of extracting knowledge on the behaviour of the Stark shift through analyzing the result of the XUV emission wavefront. This method is an interesting line of research as the Stark shift is difficult to measure for many atomic states.



Key words

atomic physics, stark shift, coherent control, XUV optics, nonlinear optics

Classification system and/or index terms (if any)

| Supplementary bibliographical information | Language |
|---|---|
| | English |
| ISSN and key title<br>0281-2762<br>Lund Reports on Atomic Physics, LRAP-572 | ISBN<br>978-91-7895-954-9 (print)<br>978-91-7895-953-2 (pdf) |
| Recipient's notes | Number of pages: 73<br>Price<br>Security classification |

# Extreme Ultraviolet Light Shaping and Spectroscopy through Opto-Optical Modulation

by Anna Olofsson


LUND
UNIVERSITY

A licentiate thesis at a university in Sweden takes either the form of a single, cohesive research study (monograph) or a summary of research papers (compilation thesis), which the licentiate student has written alone or together with one or several other author(s).

In the latter case the thesis consists of two parts. An introductory text puts the research work into context and summarizes the main points of the papers. Then, the research publications themselves are reproduced, together with a description of the individual contributions of the authors. The research papers may either have been already published or are manuscripts at various stages (in press, submitted, or in draft).

**Cover illustration front:** The upper plot is the experimental results of shaping extreme ultraviolet light with infrared light, and the lower plot is the simulation of the experiment, flipped vertically.

**Cover illustration back:** Detector image from the experimental process of extreme ultraviolet light shaping with the opto-optical modulation technique.

**Funding information:** The thesis work was financially supported by the Wallenberg Center for Quantum Technology (WACQT) funded by The Knut and Alice Wallenberg Foundation (KAW 2017.0449).



Faculty of Science, Department of Physics

ISBN: 978-91-7895-954-9 (print)
ISBN: 978-91-7895-953-2 (pdf)

Printed in Sweden by Media-Tryck, Lund University, Lund 2021

*”Research is formalised curiosity. It is poking and prying with a purpose.”*
*- Zora Neale Hurston*

# Contents

# Acronyms

**FWHM** full-width at half-maximum. 25, 26

**IR** infrared. 14, 17, 19–22, 27–29, 35

**MCP** micro-channel plate. 20–22, 32

**OOM** opto-optical modulation. 3, 4, 13–16, 21, 23, 27, 31, 32, 35–37

**SLM** spatial light modulator. 17, 35, 36

**VMI** velocity map imaging. 31, 32

**XUV** extreme ultraviolet. 3, 4, 14–22, 24–29, 31, 35–37

# List of publications

This thesis is based on the following publications, referred to by their Roman numerals:

I **Spatial control of extreme ultraviolet light with opto-optical phase modulation**
**A. Olofsson**, E. R. Simpson, N. Ibrakovic, S. Bengtsson, and J. Mauritsson
*Optics Letters*, 46, 2356-2359, 2021.

II **Probing Stark-induced nonlinear phase variation with opto-optical modulation**
E. R. Simpson, M. Labeye, S. Camp, N. Ibrakovic, S. Bengtsson, **A. Olofsson**, K. J. Schafer, M. B. Gaarde, and J. Mauritsson.
*Physical Review A.*, vol. 100, no. 2, 2019.

All papers are reproduced with permission of their respective publishers.

Publications not included in this thesis:

**Time-resolved photoelectron imaging of complex resonances in molecular nitrogen**
M. Fushitani, S. T. Pratt, D. You, S. Saito, Y. Luo, K. Ueda, H. Fujise, A. Hishikawa, H. Ibrahim, F. Légaré, P. Johnsson, J. Peschel, E. R. Simpson, **A. Olofsson**, J. Mauritsson, P. A. Carpeggiani, P. K. Maroju, M. Moioli, D. Ertel, R. Shah, G. Sansone, T. Csizmadia, M. Dumergue, N. G. Harshitha, S. Kühn, C. Callegari, O. Plekan, M. Di Fraia, M. B. Danailov, A. Demidovich, L. Giannessi, L. Raimondi, M. Zangrando, G. De Ninno, P. R. Ribič, and K. C. Prince.
*The Journal of Chemical Physics*, 154(14):144305, 2021.

**A high-repetition rate attosecond light source for time-resolved coincidence spectroscopy**

S. Mikaelsson, J. Vogelsang, C. Guo, I. Sytcevich, AL. Viotti, F. Langer, YC. Cheng, S. Nandi, W. Jin, **A. Olofsson**, R. Weissenbilder, J. Mauritsson, A. L'Huillier, M. Gisselbrecht, and C. L. Arnold.
*Nanophotonics*, 10(1):117–128, 2021.

# Acknowledgements

This licentiate thesis would not have been the same, or even been at all, without a number of people who supported me in the process.

First, I would like to thank my numerous supervisors for their contributions towards this thesis. A special thank you to my main supervisor Johan, who in 2015 thought he would get an easy but mainly administrative task of being the contact person from Lund University for a Bachelor's thesis student who did her project elsewhere - but instead ended up not only supervising me through my Bachelor's project, but also through a summer project, through my Master's thesis project, and now finally through my licentiate thesis. I truly appreciate his mentorship for all these years, he has taught me more than I could possibly fit in one acknowledgement.

Second, I want to thank current and former members of the Attosecond XUV Spectroscopy group: Samuel, who not only taught me how to work in an optics lab (alas, your forever-optimistic mood in the lab even when it takes forever to find overlap is something I believe just cannot be taught) but also made me feel welcome at the division and in the office from day one. Neven, who has a wonderful ability of being exactly as understandable as he intends: when he explains physics, I could (almost) always follow the reasoning, but when he explains nonsense at lunch break, I was just as lost as I think he wants people to be. Emma, one of the most competent experimentalists I know; I think I can count the times she did not know the answer to a lab question on the fingers of one hand. She was also the balance my learning experience in the lab needed, the order to Samuel's MacGyver.

I did not only spend time in the lab while at the division, I also had the good fortune of being placed in an office with great office mates. I am thankful for all the fun and all support when needed, and apologize for all my whining when correcting student lab reports.

All the research work would be a lot less smooth if the division was not lucky enough to have (and have had) very competent non-research staff: Anne, Jakob and Maria, who made sure administration took up as little time as possible (impressively little!) and Åke, who made me believe stereotypes about IT specialists were completely made up - until I started working elsewhere and realized how much competence it must take to make what is in most other places a mess, and just make it work smoothly.

I would also like to say thank you to the friends I made while at the division, who made happy days happier and gave support when I needed it. Among this group, a special thanks goes out to Jan for snatching me away for tea breaks filled with either nonsense or saving-the-world-level conversations (anything in between was rare).

There are also other people from outside the division without whom I would not be sane enough to write this:

- My partner Rasmus, this thesis might never have been written at all without his emotional-, reality-check-, cooking-, cleaning-, snack-delivery-,..., -support. Thank you!
- My brother, the hobby-physicist who reminds me how cool physics truly is if I momentarily forget.
- My father, for always believing in my abilities, and whose questioning mind I (un?)fortunately inherited.
- Lovisa and Mariam (Schrödinger's Kittens!), who inspire me to go for it, to try, and try again. Their support and input is often just what I need, for scientific or life struggles (plus the mojito that often comes along with said support and input).
- My friends from childhood: Maria, Julia, Hanne and Veronica, who give me perspective, honesty when needed, and so much laughter. It would be difficult to stay frustrated about being stuck on a lab problem when friends like this take you out for sushi or a run!
- My Santa Barbarians: Some of you live very far away but still managed to make me feel supported and like I could always choose to not be alone in the lab. I don't know if any of you ever understood what I did in the lab, but your virtual encouragement when I very excitedly sent Snaps of white lines moving on a dark screen as well as the virtual support when they most decidedly did not want to move, was like a hug through the many miles between us.
- And many more, that I could not fit into a category above: thank you, for making my life and my work brighter and better.

# Abstract

Extreme ultraviolet (XUV) light is a central component in many methods to study the world around us. The research fields that use XUV light span many different topics; XUV light is for example a key component when the world's shortest (at the time of writing) light pulses are produced. XUV light is typically resonant with atomic transitions from the ground state to high energy levels or ionization of an inner shell electron, which makes it a very useful tool for spectroscopy. However, this property also makes it problematic to work with XUV beams, as typical optical tools based on transmission will have their intrinsic material changed by the passage of the XUV light. It is therefore interesting to develop new control techniques for light in the XUV. In this thesis I present how XUV light can be controlled by using an atomic ensemble as control medium. An XUV pulse excites the atomic ensemble, which starts to re-radiate XUV light. The control of this emission is exerted through control of the emission wavefront. This is achieved by a second light pulse (infrared for the research this thesis is based on), that induces a Stark shift of the energy levels of the atomic ensemble. The Stark shift is intensity-dependent, thus, control of the intensity profile of the second pulse gives control of the phase modulation of the XUV emission from the atomic ensemble. This thesis is concerned partly with the possibility to shape the XUV light, also in a non-linear fashion, by controlling the intensity profile of the second pulse. However, this thesis also delves into the possibility of extracting knowledge on the behaviour of the Stark shift through analyzing the result of the XUV emission wavefront. This method is an interesting line of research as the Stark shift is difficult to measure for many atomic states.

## Populärvetenskaplig sammanfattning på svenska

Denna avhandling handlar om hur man kan kontrollera ljus som har en mycket kort våglängd, och hur resultatet av denna kontroll kan säga något om materialet som styrverktyget använder - det kan låta konstigt, men är egentligen något vi är vana vid. Det kan liknas vid att ett prisma kan dela upp vitt ljus så att man ser de olika komponenterna, och vi kan lära oss något om ljusets sammansättning, men samtidigt säger skillnaden i hur olika färger sprids något om egenskaper i prismats material som uppenbarligen är olika för olika färger. Problemet med ljuset jag har arbetat med, extrem-ultraviolett ljus, är att det är ett så bra verktyg för att studera så många olika material, det interagerar och ger information om energinivåer för i princip alla material! Men absorberas på kuppen i materialet som ofta förstörs av den höga energin. Detta är ett problem för styrningen *innan* tillfället där ljuset ska undersöka ett testmaterial, för hur formar man ljuset utan att det absorberas och förstör styrverktyget om det nu absorberas av alla material styrverktygen görs av? Detta dilemma innebär att det inte går att använda ett glasprisma, eller en vanlig lins, eller något annat styrmedel för ljus som kräver att ljuset går igenom ett material.

För att lösa dilemmat krävs det en krokodil-lösning: byt slagfält till ett du är bättre på att kontrollera! Krokodilen drar ner ett byte under vattenytan där de har ett övertag - samma idé gör det möjligt att kontrollera extrem-ultraviolett ljus genom att byta slagfält. Detta byte av slagfält innebär att man inte försöker styra det extrem-ultravioletta ljuset i sig, utan låter det absorberas av en grupp atomer och sedan kontrollerar man dem istället. Denna angreppsvinkeln fungerar i två steg: först träffar den extrem-ultravioletta ljusvågen en grupp atomer, och sätter deras elektroner i svängning runt atomkärnan. Denna svängning innebär att atomerna själva kommer börja skicka ut extrem-ultraviolett ljus. Sedan, i det andra steget, skickar man in en ljuspuls med en annan våglängd, som påverkar atomerna och hur de skickar ut ljus. På så vis kan man påverka det extrem-ultravioletta ljuset genom att kontrollera den andra ljuspulsen. Tricket här är att den andra ljuspulsen kan vara ljus med an annan våglängd, där man inte har samma problem med absorption i material.

Mitt arbete har gått ut på att undersöka hur formen på den andra ljuspulsen påverkar formen på det extrem-ultravioletta ljuset som atomerna skickar ut, och om det är möjligt att styra det extrem-ultravioletta ljuset inte bara i riktning utan även att forma det genom att forma den andra ljuspulsen. Men, jag har också arbetat med tekniken på det omvända sättet: jag har undersökt hur man kan få information om interaktionen mellan atomerna och den andra ljuspulsen genom att undersöka vad som händer med det extrem-ultravioletta ljuset atomerna skickar ut.

# Extreme Ultraviolet Light Shaping and Spectroscopy through Opto-Optical Modulation

# Chapter 1

# Introduction

This licentiatie thesis falls under the large category of scientific work that is the field of spectroscopy and spectroscopic techniques. Spectroscopy is an old field of science that concerns all interaction between matter and radiation - no wonder the field is huge! Despite its old age, the field is still relevant. Knowledge collected from spectroscopic measurements includes the vast majority of the knowledge of energy structure of matter in general and specific energy structures for each element. Knowing the energy structure of an element is important information to be able to predict how this element will behave in different situations; the energy structure is often a first clue to the structure of the electronic configurations. This structure is so crucial for the properties of an element that the elements were sorted (with a few exceptions) after their electronic structure in the periodic table already before the electronic structure was discovered, simply based on how the elements behaved in different situations.

The radiation that is used to study the energy structure of an element is typically chosen to have an energy range that matches the energy of the transition that should be studied; in other words, that the radiation is resonant with the transition. For transitions where an electron is ionized from shells close to the nucleus, the radiation in the resonant energy range is XUV light.

However, the fact that extreme ultraviolet (XUV) light is resonant with these transitions also means that it reacts very easily with all matter. This creates a problem when an experiment requires shaping or steering of an XUV beam. For light in many other wavelengths, it is possible to shape and steer a light pulse with a vast variety of optical tools. For XUV light, the user was historically restricted to mainly reflective optics. However, the technique of opto-optical modulation (OOM) offers an alternative route to be able to control XUV light. This alternative route uses funda-

mental properties of light-matter interaction to reshape XUV light as it interacts with an ensemble of atoms.

During this licentiate project I have worked on improving the OOM technique, primarily focusing on the proof-of-principle of shaping XUV light using OOM, but also on the possibility of extracting information on the behaviour of the atoms by looking at how they react to OOM.

# Chapter 2

# Light-Matter Interaction

This thesis and the research described here, is based on the fundamental properties of light-matter interaction. This chapter will therefore be devoted to describing the parts of light-matter interaction theory that are essential to the work I have done during this licentiate thesis project.

## 2.1 Classical description of light-matter interaction

The simplest description of light-matter interaction, is in my opinion the quantum mechanical description of interactions between an atom and the quantized light field where energy is traded in the form of photons. For example for absorption, the atom gains an energy that is equal to that of the photon, and the field loses an equal amount of energy. However, when dealing with many atoms and many photons, as in the research presented in this thesis, it can be more illuminating to consider light-matter interaction in a simplified classical dipole picture.

In the classical picture, light-matter interaction is treated by considering light as a wave. The force caused by the electrical field of the light accelerates the positive nucleus of an atom and its negatively charged electron cloud in opposite directions. When the electric field vector changes direction, so does the displacement force on the atom. Here, the atom could be thought of as a string or a harmonic oscillator, so that when it is put in motion, it oscillates at a certain angular frequency $\omega_0$ [1](Ch. 2A). Assuming the field is resonant gives that $\omega_{field} = \omega_0$, and it can be understood that the oscillatory motion of the atom is phase-shifted by 90° compared to the field - this is because whenever the field is positive, it pushes the electrons in the negative direction, so that the electrons are furthest away from the nucleus in the negative di-

rection when the field has been positive for as long time as possible, in other words at the point where the field crosses zero from positive to negative. Thus, a sinusoidal electric field will cause a sinusoidal displacement of the electron cloud around the nucleus, with the response field of the atom being phase-shifted by 90° to the field. The created oscillation of the electron cloud will in turn radiate its own electric field, as every accelerated charged particle will emit an electromagnetic field.

However, this is not the whole story. For the research in this thesis, macroscopic effects need to be taken into account. What this means is that nearby atoms will emit their own light fields in response to the initial light, and these electrical fields will affect the atom as well. To account for this, the integral over the fields from an infinite sheet of charges at a distance (perpendicular to the sheet) very far away is considered. The result of this integral is discussed in [2] (Ch. 30-7); for the reasoning here it is sufficient to know that accounting for other atoms leads to a response field from the atoms that has an additional phase shift of 90° (in the form of a factor $1/i$). Thus, to summarize the classical picture: in the macroscopic picture of light-matter interaction the net response field from the atoms due to the initial light field is phase-shifted by 180°[2].

An example of what this leads to is that if an incoming light field is resonant with the intrinsic frequency of the atoms, the response field will interfere destructively with the initial field due to the identical frequencies and the phase shift between them. The effect of this is absorption lines.

**Figure 2.1:** In the classical description of light-matter interaction, absorption lines can be explained by the phase shift between the incoming light wave and the light waves that are emitted from the atoms after the incoming light has caused the electrons to oscillate.

## 2.2 Light-matter interaction in a semi-classical two-level system

The fully classical picture that was presented in the previous section is useful for understanding the research of Paper I and Paper II, but for other aspects it is necessary to include the quantum nature of the atom. The picture I will use for the remaining sections of this chapter is the semi-classical picture where the light is not quantized, and is considered a wave, but the atom is quantized. To simplify, only a two-level system of the atom is considered (see Fig. 2.2).

To start describing the system mathematically, I start from the time-dependent Schrödinger equation:

$$i\hbar\frac{\partial\Psi}{\partial t} = \hat{H}\Psi \tag{2.1}$$

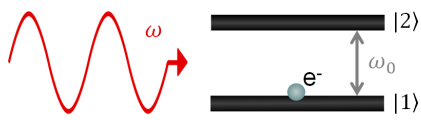


**Figure 2.2:** Description of the two-level system used to model the light-matter interaction in the semi-classical picture.

where $\hbar$ is the reduced Planck's constant, $\Psi$ denotes the wavefunction and $\hat{H}$ denotes the Hamilton operator [3](7.1). If the interaction with the external field $\hat{H}_I(t)$ is the only time-dependent effect, the Hamiltonian can be split up and written as:

$$\hat{H} = \hat{H}_0 + \hat{H}_I(t), \tag{2.2}$$

where $\hat{H}_0$ is the field-free Hamiltonian. Using the Dirac notation, a general wavefunction $\Psi(\mathbf{r}, t) = |\Psi\rangle$ can be expressed as:

$$|\Psi\rangle = c_1(t)|1\rangle e^{-i\omega_1 t} + c_2(t)|2\rangle e^{-i\omega_2 t}, \tag{2.3}$$

where $|j\rangle$, $j = 1, 2$ are the time-independent, position-dependent eigenfunctions of $\hat{H}_0$ with eigenvalues $E_j = \hbar\omega_j$, and the coefficients $c_j(t)$ fulfill that the probability of finding the system in the state $|j\rangle$ is $|c_j(t)|^2$ [3](Ch. 7.1).

Further simplifications can be made by using that the absolute value of the energy levels in the system is free to redefine, and the energies of the two-level system therefore can be set to zero and $\hbar\omega_0$:

$$|\Psi\rangle = c_1(t)|1\rangle + c_2(t)|2\rangle e^{-i\omega_0 t} \tag{2.4}$$

With this change of absolute value for the energy levels, the unperturbed Hamiltonian can be written [1](Ch 2.3):

$$\hat{H}_0 = \hbar\begin{pmatrix} 0 & 0 \\ 0 & \omega_0 \end{pmatrix}. \tag{2.5}$$

For the next step, which is to describe the interaction Hamiltonian for a monochromatic external field, two things are very useful. The first is to use a technique called the Göppert Mayer gauge to describe the potentials of the electromagnetic field. The second is to assume that the wavelength of the field is much longer than the span of the atom, and that it is therefore approximately correct to say that the field potentials at the position of the electron $\mathbf{r}$ are the same as those at the atomic center of mass

$\mathbf{r}_0$. With these two points fulfilled, the interaction Hamiltonian can be described [1] (Ch. 2.3):

$$\hat{H}_I(t) = e(\hat{\mathbf{r}} - \mathbf{r}_0) \cdot \mathbf{E}_0(\mathbf{r}_0)\cos(\omega t + \phi), \tag{2.6}$$

where $e$ is the elementary charge, $\omega$ is the angular frequency of the field and $\mathbf{E}_0(\mathbf{r}_0)$ is the electric field amplitude at position $\mathbf{r}_0$. If the polarization of the field is assumed to be along $\hat{x}$, the interaction Hamiltonian can be rewritten into:

$$\hat{H}_I(t) = eE_0(\mathbf{r}_0)\hat{x}\cos(\omega t + \phi). \tag{2.7}$$

Combining Eq. 2.4 and Eq. 2.7 gives:

$$\begin{aligned}\langle\Psi|\hat{H}_I|\Psi\rangle = eE_0(\mathbf{r}_0)\cos(\omega t + \phi)\cdot \\ \left[|c_1|^2\langle 1|\hat{x}|1\rangle + c_1c_2^*\langle 2|\hat{x}|1\rangle \mathrm{e}^{i\omega_0 t} + c_1^*c_2\langle 1|\hat{x}|2\rangle \mathrm{e}^{-i\omega_0 t} + |c_2|^2\langle 2|\hat{x}|2\rangle\right].\end{aligned} \tag{2.8}$$

The integral $\int_{-\infty}^{\infty}\Psi_j^*\mathbf{r}\Psi_j d\mathbf{r}$ is an integral over all space of an odd function and is therefore zero [1](Ch. 2B), thus:

$$\begin{aligned}\langle\Psi|\hat{H}_I|\Psi\rangle = eE_0(\mathbf{r}_0)\cos(\omega t + \phi)\cdot \\ \left[c_1c_2^*\langle 2|\hat{x}|1\rangle \mathrm{e}^{i\omega_0 t} + c_1^*c_2\langle 1|\hat{x}|2\rangle \mathrm{e}^{-i\omega_0 t}\right].\end{aligned} \tag{2.9}$$

Introducing the Rabi frequency $\Omega \equiv \frac{e\langle 1|\hat{x}|2\rangle E_0(\mathbf{r}_0)}{\hbar}$ gives:

$$\langle\Psi|\hat{H}_I|\Psi\rangle = \hbar\left[c_1c_2^*\Omega^*\mathrm{e}^{i\omega_0 t} + c_1^*c_2\Omega\mathrm{e}^{-i\omega_0 t}\right]\cos(\omega t + \phi). \tag{2.10}$$

Finally rewriting the cosine term to exponential form gives:

$$\begin{aligned}\langle\Psi|\hat{H}_I|\Psi\rangle = \hbar c_1c_2^*\frac{\Omega^*}{2}\left(\mathrm{e}^{i((\omega+\omega_0)t+\phi)} + \mathrm{e}^{-i((\omega-\omega_0)t+\phi)}\right) \\ + \hbar c_1^*c_2\frac{\Omega}{2}\left(\mathrm{e}^{i((\omega-\omega_0)t+\phi)} + \mathrm{e}^{-i((\omega+\omega_0)t+\phi)}\right).\end{aligned} \tag{2.11}$$

The full Hamiltonian can then be expressed in matrix form as:

$$\hat{H} = \hbar\begin{pmatrix} 0 & \frac{\Omega}{2}\left(\mathrm{e}^{i((\omega-\omega_0)t+\phi)} + \mathrm{e}^{-i((\omega+\omega_0)t+\phi)}\right) \\ \frac{\Omega^*}{2}\left(\mathrm{e}^{i((\omega+\omega_0)t+\phi)} + \mathrm{e}^{-i((\omega-\omega_0)t+\phi)}\right) & \omega_0 \end{pmatrix}. \tag{2.12}$$

The evolution can be described in two different cases, one quasi-resonant where $|\omega - \omega_0| << \omega_0$, and a non-resonant case. For the opto-optical modulation technique that is used in both Paper I and Paper II, both the quasi-resonant case and the non-resonant case are important.

### 2.2.1 Rabi oscillations

If the field is quasi resonant with the energy separation between $|1\rangle$ and $|2\rangle$, so that $|\omega - \omega_0| << \omega_0$, then the terms dependent on $\mathrm{e}^{\pm i((\omega+\omega_0)t+\phi)}$ will oscillate much faster than the terms dependent on $\mathrm{e}^{\pm i((\omega-\omega_0)t+\phi)}$. Also, when integrating the temporal evolution during an interaction period, the terms dependent on $\mathrm{e}^{\pm i((\omega+\omega_0)t+\phi)}$ will have a factor $(\omega+\omega_0)^{-1}$ that suppresses them compared to the other terms. This means that the effect of these terms can be neglected; this approximation is the rotating wave approximation [3](Ch 7.1). The temporal evolution of $c_1$ and $c_2$ can then be described as [3] (Ch 7.3):

$$i\frac{d}{dt}c_1 = c_2\frac{\Omega}{2}\mathrm{e}^{i(\delta t+\phi)} \tag{2.13}$$

and

$$i\frac{d}{dt}c_2 = c_1\frac{\Omega^*}{2}\mathrm{e}^{-i(\delta t+\phi)}, \tag{2.14}$$

where the detuning $\delta = \omega - \omega_0$ is introduced.

To see the effect of the field on the populations in the two-level system, Eq. 2.13 and Eq. 2.14 can be combined into a differential equation:

$$i\frac{d^2}{dt^2}c_2 = \frac{\Omega^*}{2}\left[\left(\frac{dc_1}{dt}\right)\mathrm{e}^{-i(\delta t+\phi)} + c_1\mathrm{e}^{-i(\delta t+\phi)}\left(-i\delta\right)\right] \Leftrightarrow$$

$$i\frac{d^2}{dt^2}c_2 = \frac{\Omega^*}{2}\left[\left(-ic_2\frac{\Omega}{2}\mathrm{e}^{i(\delta t+\phi)}\right)\mathrm{e}^{-i(\delta t+\phi)} + \left(i\frac{dc_2}{dt}\frac{2}{\Omega^*}\mathrm{e}^{i(\delta t+\phi)}\right)\mathrm{e}^{-i(\delta t+\phi)}\left(-i\delta\right)\right] \Leftrightarrow$$

$$\frac{d^2}{dt^2}c_2 = -\left|\frac{\Omega^*}{2}\right|^2 c_2 + \frac{dc_2}{dt}\left(-i\delta\right) \Leftrightarrow$$

$$\frac{d^2}{dt^2}c_2 + \frac{dc_2}{dt}\left(i\delta\right) + \left|\frac{\Omega}{2}\right|^2 c_2 = 0. \tag{2.15}$$

Eq. 2.15 has a solution such that the population of the upper level can be found as [3] (Ch. 7.3):

$$|c_2(t)|^2 = \frac{\Omega^2}{\Omega^2+\delta^2}\sin^2\left(\frac{\sqrt{\Omega^2+\delta^2}t}{2}\right). \tag{2.16}$$

For $\delta \to 0$, the effect of the field is thus to cycle the population between the two levels. This is called Rabi oscillation, hence the term "Rabi frequency" for $\Omega$. As can be seen from Eq. 2.16, the larger the detuning gets, the smaller the fraction of the population that is transferred for each cycle becomes.

### 2.2.2 Stark effect

Another light-matter interaction effect that is crucial for the research in Paper I and Paper II is the Stark effect. It describes how an external field changes the atomic energy level structure [4]. To see where this effect comes from, it is necessary to rewrite Eq. 2.13 and Eq. 2.14 taking into account the non-resonant terms that were neglected in the previous section. If the external field phase $\phi$ is assumed to be zero:

$$i\frac{d}{dt}c_1 = c_2\frac{\Omega}{2}\left(\mathrm{e}^{i\delta t} + \mathrm{e}^{-i(\omega_0+\omega)t}\right) \tag{2.17}$$

and

$$i\frac{d}{dt}c_2 = c_1\frac{\Omega^*}{2}\left(\mathrm{e}^{-i\delta t} + \mathrm{e}^{i(\omega_0+\omega)t}\right). \tag{2.18}$$

For non-resonant fields, and if the field is weak, a perturbative assumption helps finding a solution. If the Rabi frequency is real, $\Omega^* = \Omega$, a perturbative solution to these coupled equations can be found as [1](Ch 2.3.4):

$$c_2(t) = \frac{\Omega}{2}\left(\frac{\mathrm{e}^{-i\delta t}}{\delta} - \frac{\mathrm{e}^{i(\omega+\omega_0)t}}{\omega+\omega_0}\right)c_1(t). \tag{2.19}$$

For this case, the time derivative of the lower state is useful to look at as an example:

$$i\frac{d}{dt}c_1 = \left(\frac{\Omega}{2}\left(\frac{\mathrm{e}^{-i\delta t}}{\delta} - \frac{\mathrm{e}^{i(\omega+\omega_0)t}}{\omega+\omega_0}\right)c_1\right)\cdot\frac{\Omega}{2}\left(\mathrm{e}^{i\delta t} + \mathrm{e}^{-i(\omega_0+\omega)t}\right) \quad \Leftrightarrow \tag{2.20}$$

$$i\frac{d}{dt}c_1 = \frac{\Omega^2}{4}\left(\frac{1}{\delta} - \frac{\mathrm{e}^{i2\omega t}}{\omega+\omega_0} + \frac{\mathrm{e}^{-i2\omega t}}{\delta} - \frac{1}{\omega+\omega_0}\right)c_1. \tag{2.21}$$

The two terms in the middle of Eq. 2.21 are oscillating rapidly, and do not contribute to the Stark effect. The two remaining terms are both constant. Given Eq. 2.1 and Eq. 2.12, it is clear that a constant shift of the temporal derivative of a coefficient that depends only on that same coefficient belongs to the diagonal of $\hat{H}$, and can thus be interpreted as a shift of the energy level of the evaluated state. This energy shift does occur and was first reported already in 1913 [4]. To simplify Eq. 2.21 further, it can be seen that the first term is the most important, since the denominator $\delta$ is smaller than $\omega + \omega_0$. Thus the Stark shift of the atomic energy level from a non-resonant external field (using a perturbation approximation) can be written:

$$\Delta E_{Stark} \approx \frac{\Omega^2}{4\delta}. \tag{2.22}$$

From Eq. 2.22 it can be seen that the Stark shift depends on the sign of the detuning, and on the intensity of the field since $\Omega$ is proportional to the field amplitude [1](Ch.2.3.4).

The expression above is valid for a non-resonant and weak external field. This is not the only system where an approximate solution can be found. If a system with an electron very far out from the nucleus is considered, then an expression for the energy shift experienced by the electron due to the field can be obtained. If the assumption that the electron is far away from the nucleus is taken to its extreme, the situation can be reduced to a free electron oscillating in an electric field. The energy gained by the electron is then the average of the kinetic energy of the oscillatory motion, which is commonly called the ponderomotive energy $U_p$ [5, 6]. The ponderomotive shift is given by:

$$U_p = \frac{e^2 \mathbf{E}_0^2}{4 m_e \omega^2}, \tag{2.23}$$

where $e$ is the elementary charge and $m_e$ is the mass of the electron. It can be seen that also in this situation, the energy shift is proportional to the intensity of the external field.

# Chapter 3

# Opto-Optical Modulation

An experimental technique that has been crucial to the research of this licentiate project is OOM, which allows light to be controlled using phase modulation created by another light pulse. This chapter will go through the technique in detail, starting from the concept of controlling electromagnetic radiation by controlling the wavefront.

## 3.1 Steering using phase

Radar is perhaps the most commonly known example of how electromagnetic radiation can be steered by controlling its phase. An array radar is made up of many antennas, with each antenna emitting a signal that interferes with the rest (see Fig. 3.1). If all antennas are in phase, as in Fig. 3.1b, then the interference between the different antennas will ensure that the parts of the radiation field from a single antenna that are not travelling upward in the figure will be suppressed [1]. This results in a wavefront that is horizontal. If a position-dependent phase shift is added, the amplitude crests of the radiation field from one antenna will be slightly off compared to the crests of the radiation from its neighbour. If the phase shift increases incrementally for each antenna, and their positions are equally spaced, the phase shift will result in a tilted wavefront across the antenna field as depicted with exaggeration in Fig. 3.1c. This means that the travelling direction for the radiation where the emission will not be cancelled out by destructive interference will have a slight angle compared to the previous emission direction.

[1] The seemingly spherical radiation field from an antenna such as the one depicted is not entirely correct, it is a simplification made for the sake of the analogy.

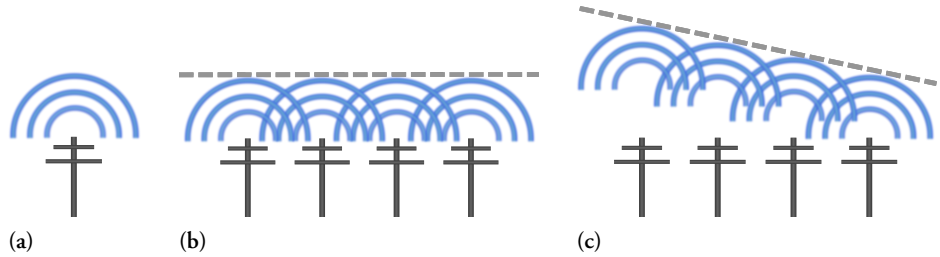


**Figure 3.1:** Schematic description of how the phase difference between adjacent radar antennas can be used to steer radar emission from a phased array radar. The blue lines represent some of the wavecrests of the electromagnetic radiation from an antenna, and the dashed gray lines mark the direction of the wavefront.

Radar is not the only example of how control of the phase and the wavefront can be used to control light, the same principles apply for example for a lens, as seen in Fig. 3.2. The wavefront will be shaped in a way that depends on which direction the lens is curved: if the middle of the lens is thicker than the edges, the optical path through the middle will be longer than the path through the edges, and the part of the wave that propagates through the center will be delayed compared with the parts at the edges. This leads to the beam being focused.

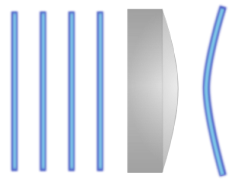

**Figure 3.2:** The curving of the wavefront (blue lines) in a positive lens creates a focusing effect.

OOM uses the same principle to control light as radar does, but OOM replaces the antennas with atoms. The basic idea of the technique is that the wavefront of incoming XUV light is modified by modifying the phase of the response field (see section 2.1) when the light has interacted with a gas [7], as described schematically in Fig. 3.3. The steps in detail, depicted in Fig. 3.3 are as follows: first, an XUV pulse excites a manifold of atomic states and the superposition between the excited states and the ground state starts to oscillate (see section 2.2.1). The phase of the superposition evolves with $\omega_0 t$, where $\hbar\omega_0$ as previously is the difference in energy between an excited state and the ground state. Step two is that the atoms after the excitation start emitting XUV light, as discussed in section 2.1. After a variable time delay, the third step occurs. This is when a second pulse, the IR control pulse, is sent onto the atoms and the induced Stark-shift modifies the energy of the states in the superposition. From Eq. 2.4, it can be seen that the energy difference ($\hbar\omega_0$) between the states will affect the phase evolution. Therefore, the induced Stark shift modifies also the phase evolution of the superposition, and therefore also the wavefront of the light that is emitted from the atoms. During the time the IR pulse interacts with the atoms, a phase shift (compared to the evolution without the interaction with the control pulse) is accumulated, and

this shift remains also when the pulse has passed and the phase evolves unaffected. The control pulse should be non-resonant to the transitions that were excited by the XUV pulse, thus affecting the atoms mainly through Stark-shifting the energy levels. The effect on the phase during this step will be:

$$\frac{d\phi}{dt} = \omega_0 + \frac{\Delta E_{Stark}}{\hbar} \tag{3.1}$$

where $\Delta E_{Stark}$ is the shift of the energy separation between the states in the superposition due to the Stark effect.

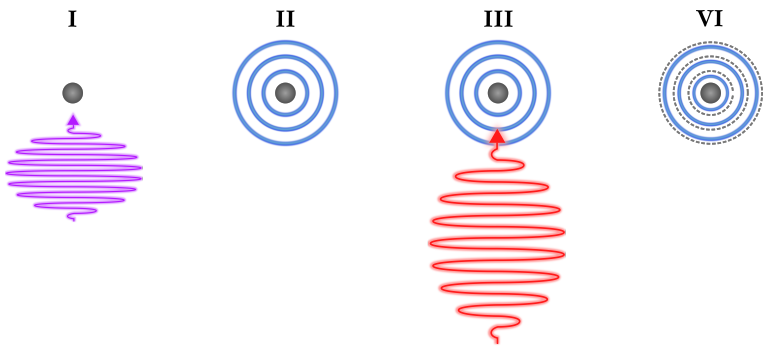


**Figure 3.3:** Schematic description of the opto-optical modulation process. In step I, an initial XUV pulse excites the atom. In step II, during an adjustable time delay, the atom will emit XUV light that is out-of-phase with the initial pulse. In step III, a non-resonant control pulse is sent onto the atom. This will Stark-shift the energy levels of the atom and change the phase of the emitted XUV light, as depicted in step IV.

However, as discussed in Sec. 2.2.2, the Stark shift is intensity-dependent. If the intensity of the control pulse varies across the ensemble of atoms, the Stark shift will vary as well. This means that the Stark shift can be used to create a situation like that of Fig. 3.1c, with atoms replacing the antennas (see Fig. 3.4). A major difference is that the emission from the atoms contains many frequencies from many different transitions. This is both because the initial XUV pulse has a broad frequency span, and because the atoms have many transitions in this particular frequency region. The Stark shift is state-specific, meaning that when I discuss the phase modulation using OOM, I mean the emission from one specific transition. To be more precise, it is possible to set up a relation for the total phase shift for each transition and position $r$ in the atomic ensemble due to the Stark shift:

$$\Delta\phi(r) = \frac{1}{\hbar}\int_{T_2} \Delta E_{Stark}(r,t)dt \tag{3.2}$$

where $T_2$ is the pulse duration of the non-resonant control pulse. If the temporal shape of the control pulse is known, the integral over the pulse duration can be calculated. The spatial shape of the phase shift will thus be dependent on the spatial shape

of the intensity of the control pulse, and here one interesting aspect of the technique appears: it is not only possible to apply a linear phase shift across the ensemble and steer XUV light, as depicted in Fig. 3.4, but it is also possible to shape it.

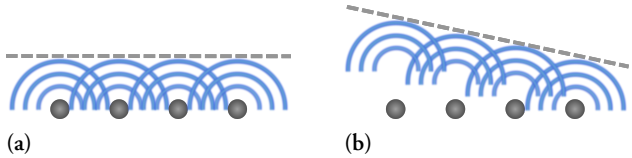


**Figure 3.4:** Schematic description of how the phase difference between adjacent atoms can be used to steer XUV emission from an atomic ensemble. The blue lines represent some of the wavecrests of the XUV light from an atom, and the dashed gray lines mark the direction of the wavefront.

## 3.2 Shaping extreme ultraviolet light using opto-optical modulation

The principle behind the shaping of XUV light using OOM is the same as any optical instrument making changes in the near-field that are meant to change the far-field in a specific way. The principle is rather counter-intuitive, but the main idea is that the near-field will be shaped like the Fourier transform of the far-field [8].

Fig. 3.5 gives a few examples of how the application of a control pulse can shape the XUV light in the far-field. In the figure, a linear relationship is assumed between the intensity of the control pulse and the phase shift. This would be the case if the situation concerns an electron that is not tightly bound to a nucleus, meaning that the behaviour of the electron approaches that of a free electron and thus the Stark shift approaches the ponderomotive shift (see Eq. 2.23).

Two examples from Fig. 3.5 are especially important for Paper I and Paper II; that of a linearly varying control pulse intensity across the atomic ensemble, and that of a Gaussian intensity shape of the control pulse. First, I will focus on the latter case, which is important for Paper I, and the second case will be the focus of Sec. 3.3.

Fig. 3.5d shows that the XUV intensity profile has fringes in the far-field when imprinted with the phase shift from a Gaussian control pulse. These fringes are an interference effect due to multiple points in the near-field having the same phase gradient after the control pulse has been applied. This means that the emission from these points will be directed to the same point in the far-field. However, the absolute value of the phase is not the same for both points, as seen in Fig. 3.6. This leads to an interference pattern in the far-field.

This was detected experimentally in Paper I, and the study is the first to show shaping

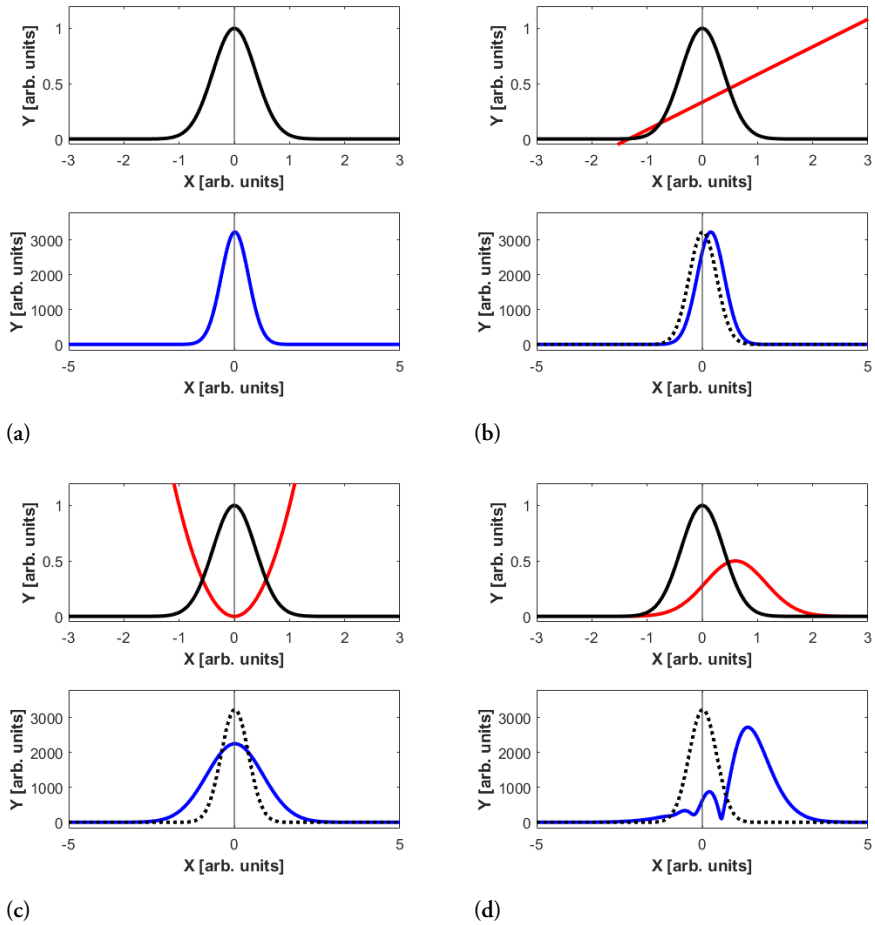


**Figure 3.5:** Examples of how an added phase shift can change the far-field of a pulse that has a Gaussian intensity profile in the near-field (upper plots). The black line denotes the near-field intensity, the red line denotes a (scaled to fit) phase that is added to the Gaussian pulse, the blue line denotes the far-field intensity and the dotted black line is the far-field of the Gaussian pulse when no phase shift has been added, for clarity.

of the spatial XUV profile using the spatial intensity profile of another light pulse. Given the possibility to shape light of certain wavelengths, for example infrared (IR), with widely available optical tools like acousto-optic modulators or spatial light modulators (SLMs) [9], this is an interesting opportunity; it allows a user to choose a shape they want for the XUV, and then tailor a light pulse of a more manageable wavelength to the needed shape to get the appropriate phase shift in the near-field.

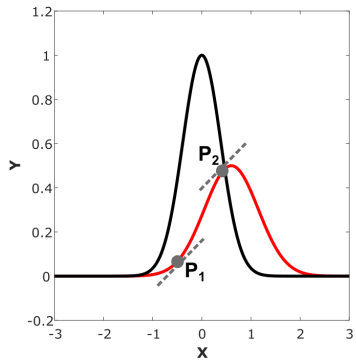


**Figure 3.6:** A pulse with a Gaussian intensity profile (black) has a Gaussian phase shift (red, scaled to fit in plot) imprinted onto it. The points $P_1$ and $P_2$ have the same phase gradient and the intensity of the Gaussian pulse in these locations will therefore be sent to the same $x$-position in the far-field. However, the absolute phase is different for the two points and this will cause interference in the far-field.

## 3.3 Using opto-optical modulation to probe the Stark effect

The case of a linearly varying control pulse intensity is interesting from an opposite perspective compared to Fig. 3.5d. If it is assumed that the intensity profile of the control pulse is linearly varying across the ensemble, and the Stark effect of a specific state is unknown, then the XUV intensity profile in the focus instead contain clues on the Stark shift. For example, if the XUV intensity shape is known and the phase variation is linear, but the far-field profile is shifted to another direction than that expected - then it can be deduced that the Stark shift has a different sign than expected.

This example can be taken one step further to coincide with what happens in Paper II: if the far-field profile is at first shifted to one direction, then the other when the control pulse intensity is increased, then the intensity value where the change in direction occurs clearly marks a region of highly non-linear behaviour of the Stark effect of the atomic state.

# Chapter 4

# Experiments

This chapter describes the experimental equipment and procedures of Paper I and Paper II, both those that took place in the laboratory and those that were computer-made.

## 4.1 Opto-optical modulation laboratory experiments

The experimental setup that was used for the studies presented in Paper I and Paper II is a tabletop pump-probe setup (see Fig. 4.1) that is described in detail in published literature [10]. The light source is a titanium-sapphire laser with a tunable wavelength in the IR (specifically around 800 nm), that after amplification and compression with chirped pulse amplification [11] delivers pulses of about 2-3 mJ with a pulse duration of about 20 fs to the setup. The repetition rate for the system is 1 kHz. This beam is split by passage through or reflection on an annular mirror, and the resulting two beams from there on follow the path of one arm each in a stabilized interferometer. A mirror on a controllable piezo-stage allows for control of the delay between the pump and the probe pulse with high precision. The pump pulse path directs the pump pulse into a gas jet with a pulsed valve, where the IR pump pulse is used to generate XUV light. The generation occurs through a nonlinear process that generates odd high-order harmonics of the laser frequency, yet without the drop-off in intensity with increasing order that occurs for lower orders [12–17]. A variable aperture allows for control of how much IR intensity is used to generate the XUV light.

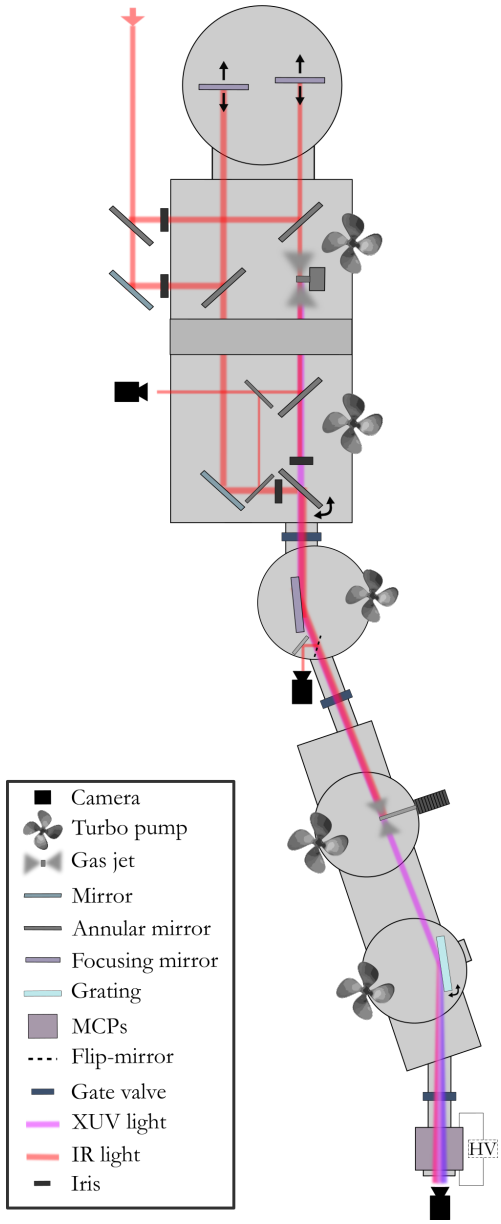


**Figure 4.1:** Schematic description of the setup used for the laboratory experiments. Ultrashort IR pulses are divided by an annular mirror, which marks the start of an interferometer. The annular part of the initial IR pulse is used to excite a gas in a non-linear process that creates XUV light. The XUV light then propagates further and becomes the pump in a pump-probe procedure where the target is the atomic ensemble of the second (lower in figure) gas jet. The probe is the remaining part of the initial IR pulse and interacts with the target ensemble a variable time delay after the pump. The delay is controlled through moving the focusing mirror of the probe beam with its piezo-driven linear stage (upper circular chamber in the figure). The leftmost camera provides active stabilization through monitoring changes in the interference pattern formed by the two arms of the interferometer, and then correcting the changes through controlling the linear stages supporting the focusing mirrors in the upper chamber. The center camera is used to view the spatial overlap of the two pulses in the focus. Finally the rightmost camera is used to record the emission from the target ensemble, which is amplified by MCPs.

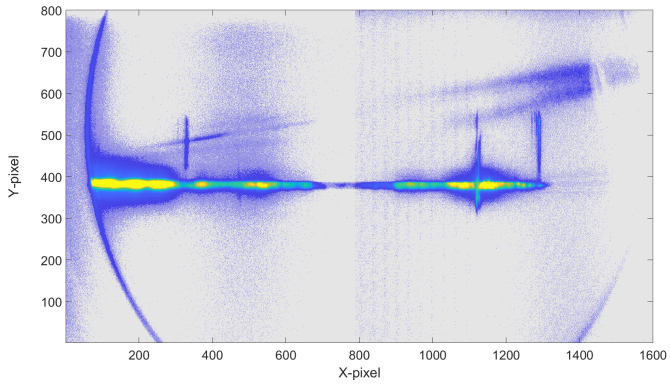


**Figure 4.2:** Example of a false-color spectrum captured by the camera of the setup. The x-axis is frequency-separated due to a grating before the detector, while the y-axis shows the intensity distribution of the XUV light across the vertical direction. The horizontal regions of high intensity on-axis (on-axis approximated to Y-pixel≈390) hints at the frequency distribution in the form of odd high-order harmonics of the laser frequency. The harmonics are widened by the strong intensity of the fundamental pulse.

The generated XUV pulse is then recombined with the probe pulse by the passage through (for the XUV pulse) or reflection on (for the IR probe pulse) a controllable annular mirror, and focused by a toroidal mirror into a second, identical, gas jet (referred to as the target gas jet). This is where the OOM takes place, with the probe pulse serving as the non-resonant control pulse. A variable aperture in the probe arm allows for control of the intensity of the probe pulse. The controllable x-y tilt of the recombination annular mirror is used to position the probe pulse in relation to the XUV pulse to optimize the modulation of the far-field. To get as much separation between the light that is not modulated (”on-axis”) and the light that has been modulated with OOM, it is ideal to place the probe pulse so that its steepest intensity gradient overlaps spatially with the peak of the XUV intensity, as this is the place where the highest amount of atoms will be excited by the XUV pulse and therefore will be emitting a response field. The steep intensity gradient of the IR pulse will ensure that the re-direction of the emission from the on-axis XUV light is maximal. A visual guide to the concept of on-axis and modulated XUV light can be found in Fig. 4.2: this is a false-color image from the camera that detects the XUV light. In for example the right upper corner it is clear that some of the XUV has been re-directed from its original on-axis direction where a majority of the light hits the detector, as a consequence of the OOM.

The detection of the XUV light that is emitted from the atoms in the target gas jet is done by frequency separation with a reflection grating, micro-channel plates (MCPs), a flourescent screen and a camera. The MCPs basically consist of many electron multiplier tubes [18]. This means that when an XUV photon hits one of the tubes, it sets an electron free and the electron is accelerated through the tube by using an external

bias, which means it can knock out more electrons from additional surfaces, which can then be accelerated and so on, until the electron cascade reaches the phosphor screen. This means that the signal that can be seen on the camera or the phosphor screen is significantly amplified by the MCPs.

The stabilization of the interferometer is done through taking small sections of the pump and the probe pulses and recombining them onto a camera, where any instability is seen as a fluctuation of the interference pattern. These fluctuations are monitored and sent into a feedback system to the piezo stage that controls the delay between the pulses so that the changes that cause the fluctuation of the interference pattern can be compensated for.

### 4.1.1 Experimental procedure

The first step in the experimental procedure is optimizing a number of parameters: the first being the IR pump pulse intensity into the generation gas jet, to maximize XUV light generation and without getting an XUV intensity reduction due to ionizing. The second optimization is the intensity and position of the IR probe pulse with respect to the XUV pulse in the target gas, as mentioned in the previous section. The IR intensity gradient of the probe pulse (acting as the control pulse for OOM) needs to be sufficiently large to ensure that the modulated XUV is well separated from the on-axis light. After the control pulse intensity optimization, it can be beneficial to again adjust the intensity of the IR pump pulse in order to blue-shift the high-order harmonics making up the XUV pulse [19] so that the energy of a specific transition in the target gas can be matched by a shifted harmonic. This is the case for example in Paper II, where the blue-shift pushed one harmonic into resonance with the ground state $1s^2$ to $1s2p$ transition in Helium. As seen in Eq. 2.16, the transition probability is highest at resonance and therefore it leads to a stronger spectral line for this transition if the spectrum is blue-shifted into resonance.

For both Paper I and Paper II, the interesting effect to study was what happened when the probe pulse aperture was changed. In Paper II this is interesting because the changed aperture opening gives a change in intensity, which is necessary to probe the behaviour of the Stark effect as a function of the non-resonant field strength. For Paper II also the change in shape of the control pulse is crucial, as it allows change of the shape of the emission wavefront.

### 4.1.2 Data analysis

The images of the spectrum that are captured by the camera are first treated by converting the x-axis of the spectrum to frequency from wavelength, and then the effects of the nonlinear relation between wavelength and frequency on the binning of the x-axis is corrected for by interpolating, such that the x-axis remains linear. The reflection grating should provide a flat-field spectrum so that this is the only treatment necessary, but if the energy calibration of the spectrum is crucial further treatment is needed. Corrections to the energy calibration are made through using known spectral lines of the target gas, and calibrating the x-axis such that these lines coincide with each other in a way that corresponds to published spectra of the target gas[1].

To produce plots that describe the result of OOM with changing aperture opening, the spectrum for each aperture opening is treated by integrating over the energy region that correspond to the state(s) that is(are) being studied for each divergence angle.

## 4.2 Opto-optical modulation simulation description

To better understand the results from the experiments explained in the previous section, a program was written to simulate the experimental process. The model is not a comprehensive mirror image of everything that goes on in the laboratory set-up, but was written to single out the significant processes for the experimental results. The model is based on Gaussian pulses and Fourier optics. The temporal aspect of the light pulses is not considered more than by a multiplication factor into the calculated accumulated phase for each control pulse intensity.

The first step in the model is to simulate the effect of the aperture on the spatial pulse profile of the control pulse. This is done by a pass/no-pass filter set to a variable radius to mirror the variable aperture opening in the experiment. This step is depicted schematically in row I of Fig. 4.3.

The next step in the model is a far-field transform [8](Ch. 4) that simulates propagation of the control pulse from immediately after the aperture (considered the near-field) to the focus. The far-field transform is based on the Fraunhofer approximation

$$z >> \frac{k\left(x_n^2 + y_n^2\right)_{max}}{2}, \tag{4.1}$$

where $z$ is the distance between the center of the near-field active region to the center

[1]The structure of the odd-harmonic spectrum should be an easier way to calibrate the energy, however blue-shifting both disrupts the energy structure and widens the frequency span of each harmonic.

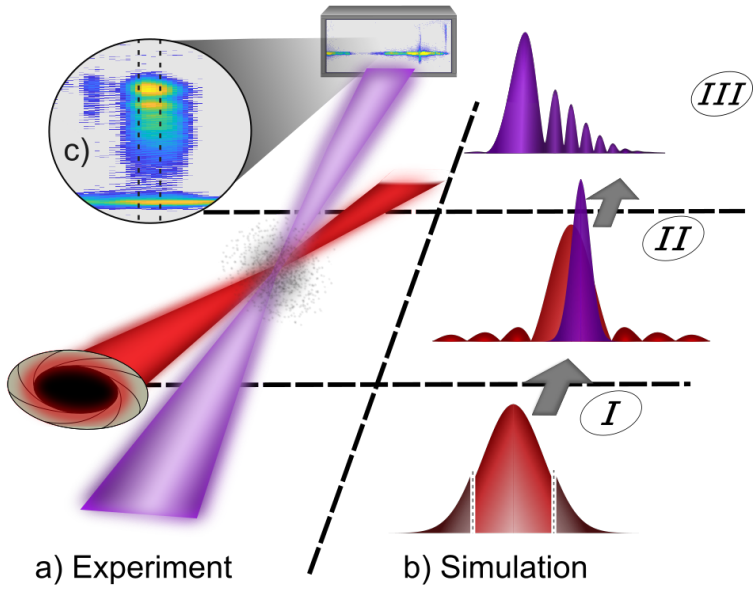


**Figure 4.3:** Comparison between the laboratory experiment setup (a) and the programmed model (b). In row I, the control pulse is cut by a variable aperture, which is simulated by a filter. In row II, the XUV emission from an ensemble of atoms is phase-modulated through the Stark-shift from the control pulse. In the simulation, this is mirrored by adding a phase shift that is calculated for each intensity, either by using an approximation of ponderomotive behaviour with control pulse intensity (Paper I), or by solving the coupled Maxwell wave equation and time-dependent Schrödinger equation (Paper II). Finally, in row III the far-field distribution of the modulated XUV emission from the atoms is detected. The grating in the experiment is omitted from the figure. The dashed lines in the spectrum (c) marks the frequency area that is integrated over to produce Fig. 4.4a.

of the far-field active region, $k$ is the wavenumber, and $\sqrt{x_n^2 + y_n^2}$ is the distance from an evaluated point to the center of the near-field (in the plane orthogonal to $z$).

Given that Eq. 4.1 holds, the propagated field $E_f(x_f, y_f)$ can be described from the known near-field $E_n(x_n, y_n)$:

$$E_f(x_f, y_f) = \frac{e^{ikz} e^{i\frac{k}{2z}\left(x_f^2 + y_f^2\right)}}{i\lambda z} \int\int_{-\infty}^{\infty} E_n(x_n, y_n) e^{-i\frac{2\pi}{\lambda z}\left(x_f x_n + y_f y_n\right)} dx_n dy_n. \tag{4.2}$$

The integral is the Fourier transform of the near-field intensity profile, evaluated at "frequencies" of $\frac{x_f}{\lambda z}$ and $\frac{y_f}{\lambda z}$. In the model, only one dimension is simulated. This is because the experiment only has one important dimension for the phase modulation; the direction that is parallel to the slits of the reflection grating. The resolution of another dimension is traded for frequency resolution.

The control pulse intensity profile that is propagated to the focus is then used to calculate the phase shift that should be added to the phase of the XUV intensity profile.

For Paper I, the energy shift was assumed to follow the ponderomotive relation in Eq. 2.23. For Paper II, collaborators from Louisiana State University performed a more detailed calculation where they solved the coupled Maxwell wave equation and the time-dependent Schrödinger equation [20], and were able to extract the accumulated phase shift from the Stark effect from their solution. This extracted phase shift for a number of different control pulse intensities is interpolated in the model to find the phase shifts that correspond to the control pulse intensities in the focus. In this manner, a specific accumulated phase shift can be assigned to each position in the focus. The XUV pulse profile is created to be Gaussian, and then modified for each focus position by the phase shift for that specific position. This is depicted in row II of Fig. 4.3.

Another far-field transform, identical to the first, is used to propagate the XUV pulse to the detector plane. The result at the detector plane will thus be a plot of the intensity across one spatial dimension (similar to row III of Fig. 4.3) that corresponds to the vertical direction in the experiment (i.e. the direction in which the XUV light is modulated). This is then converted into a 2D-plot where the intensity distribution for each divergence angle from the on-axis XUV light is instead depicted as a color scale, and where the x-position denotes the filter radius, as in Fig. 4.4 b).

## 4.3 Opto-optical modulation results

The main results from Paper I are the plots presented in Fig. 4.4. The upper plot shows the spectra from the camera in the setup, integrated over frequency areas corresponding to high-energy $p$-states in Helium, as a function of the aperture opening. The high energy of the states ensure that the assumption of ponderomotive behaviour is appropriate. Interference fringes start to appear around $x = 180$, and the fringe separation gets wider with increasing aperture opening. This behaviour continues until the changes in aperture opening only concern the fringes of the pulse, where the intensity is negligible. The same behaviour is found for the modelled system in the plot below. The match between the two plots indicate that the geometrical properties simulated in the model are in fact the main physical properties that give the plot in Fig. 4.4a its distinct fringe pattern.

The effect of the changing aperture opening is in part on the intensity of the control pulse, but also on the full-width at half-maximum(FWHM). By varying these parameters, the intensity profile of the control pulse is changed. The effect of these changes on the far-field shows the expected behaviour: as the aperture opening increases, two things should, and do, occur. The intensity of the control pulse increases, resulting in a larger overall phase change between the atoms that interact with the peak of the con-

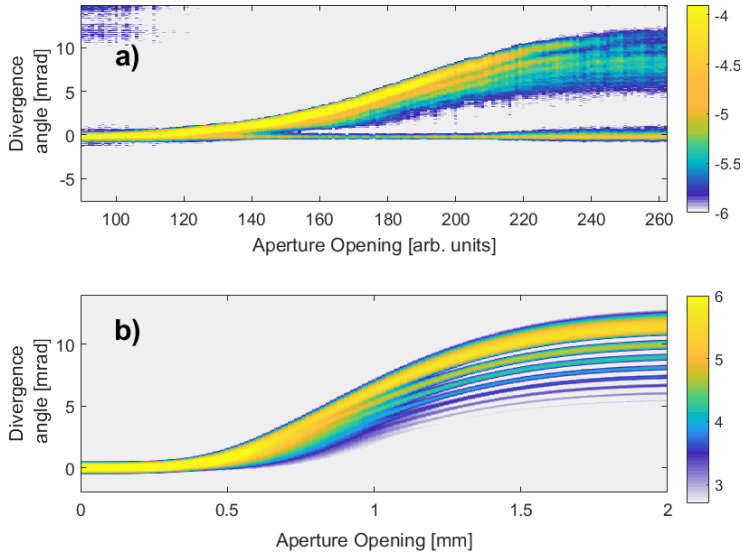


**Figure 4.4:** Results from Paper I: for a), the frequency region between the dotted lines of Fig. 4.3 c) is integrated over frequency and plotted as a function of vertical divergence angle and aperture opening. For b), the simulated result for the XUV intensity distribution in the far-field is shown as a function of pass/no-pass filter radius. The intensities are displayed in logarithmic scale.

trol pulse and those that interact with the fringes. This affects the average slope of the phase, and thus the average re-direction from the on-axis XUV light. This can be seen in an overall increasing divergence angle in Fig. 4.4. Another effect of the increasing aperture opening is that the diffraction from the opening will be less severe, and the FWHM of the control pulse intensity in the focus will be smaller. This means that the region with the emitting ensemble of atoms $\Delta y$, will span a larger part of the control pulse. This can be seen by realizing that $\Delta y$ is the area where atoms have interacted with the XUV pulse, and then comparing the overlap between the purple XUV pulse and the red control pulse in Fig. 4.3b II. When the control pulse FWHM decreases, the percentage of the control pulse that is in the active region increases, and thus there are a wider range of intensity gradients that matter for the modulation. The distance between the points with the same gradients also decreases; in Fig. 3.6 this corresponds to a reduced distance in $x$ between $P_1$ and $P_2$. This increases the distance between the fringes. This can also be seen in Fig. 4.4. There is a natural minimum in how small the FWHM of the control pulse should be, of twice the FWHM of the XUV pulse, at least if fringe visibility is concerned and as much as possible of the XUV emission from the atoms should be redirected. This is because only half of the control pulse re-directs the emission in one particular direction.

The importance of the relative position of the XUV and control pulse peaks is also

clear. As mentioned in Sec. 3.2, the visibility should be highest when the peak of the control pulse is at $x = x_0 - \mathrm{FWHM}/2$ of the XUV pulse, so that the intensity of the XUV pulse is the same for $P_1$ and $P_2$, leading to an equal number of emitters in $P_1$ and $P_2$. For a Gaussian control pulse, this coincides with when the redirection is at maximum, as the maximum IR intensity gradient overlaps with the peak of the XUV pulse. This can be seen in Fig. 4.5: the magnitude of the redirection and the fringe visibility increase as the position of the control pulse center approaches the center of the XUV pulse, but decreases when the pulse centers are too close. The symmetry follows from the symmetry of the control pulse intensity profile. Here it is also clear that the bell shape of the control pulse intensity profile matters - if the shape would have been different, the result would have been another. A triangle-shaped control pulse for example would not have resulted in fringes in a plot such as Fig. 4.5, or Fig. 4.4b. Thus, it is clear that the shape of the control pulse intensity controls the XUV intensity distribution in the far-field; OOM can indeed be used to shape XUV light.

The result presented in Paper II shows the opposite use of the OOM-technique. If it is assumed that the overlap region between the active ensemble and the control pulse is restricted to an area around $x \approx x_0 \pm \mathrm{FWHM}/2$, then the intensity gradient is approximately linear. This means that any deviation of the XUV intensity distribution in the far-field from the expected (simple displacement in the vertical direction) can be assumed to be due to a non-linear Stark shift behaviour with intensity. Such a non-linear behaviour is predicted for the transition between the ground state in Helium and $1s2p$, as seen in Fig. 4.6.

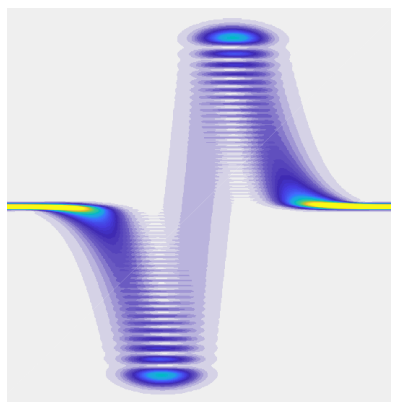

**Figure 4.5:** Simulated XUV intensity distribution in the far-field as a function of the control pulse center position in the near-field (focus plane), with the XUV pulse peak position located in the middle of the figure.

From Fig. 4.6 some observations are important for the interpretation of the experimental results: the Stark shift for the $2p$-transition is not just expected to be non-linear with intensity, but the gradient for the phase shift with intensity even changes sign. For low intensities, the intensity gradient for the $2p$-phase shift has opposite sign compared to that of the energetically higher states. Toward higher intensities though, the phase shift gradient is similar to that of the other states plotted in Fig. 4.6. This is useful for experimental purposes as it is the phase shift gradient with intensity that determines the slope of the wavefront of the XUV emission and thus the propagation direction of the modulated light (see Fig.

3.4). The distinct differences of the gradients in Fig. 4.6 thus predict distinct differences of the modulation of the $2p$ transition line compared to the transition lines of high $np$-states.

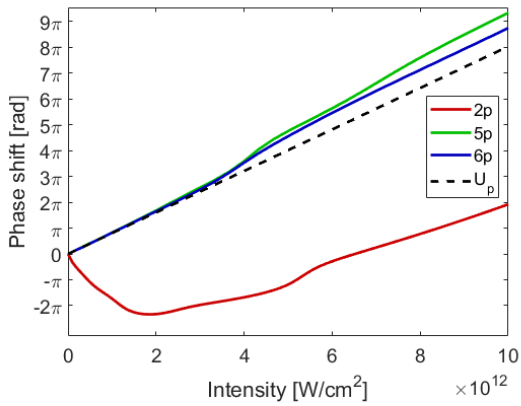


**Figure 4.6:** TDSE calculations of the accumulated phase shift due to the interaction between the ground state and the plotted different $np$-states in Helium with first a resonant light pulse (4 fs, $1 \cdot 10^{11}\mathrm{W/cm^2}$) and then, after a delay of 40 fs, with an IR pulse (27 fs, 800 nm) with varying intensity. Data corresponding to that presented in [21]. The phase shift due to the ponderomotive energy shift ($U_p$) for a free electron due to the same IR light pulse is included for comparison.

The confirmation of the theory in Fig. 4.6 by the experimental result can be perceived already in the detector picture seen in Fig. 4.7 (a zoomed-in version of Fig. 4.2). The observations from Fig. 4.6 predict different modulation directions for the $2p$-transition line compared to that of high $np$-transition lines. This is clear in Fig. 4.7, as the $2p$-transition line has been re-directed in both the positive and the negative vertical direction (seen for X-pixel≈1125), while the high $np$-transition lines only display re-direction in the positive vertical direction.

A more processed result is the divergence angle plot as a function of aperture opening for the $2p$-transition line, shown in Fig. 4.8. In the figure it can be seen that there is re-direction of the XUV light in both the positive and the negative vertical direction. The overall larger intensity of the re-direction in the positive vertical direction also implies that the phase gradient sign that corresponds to this direction of modulation is present to a higher degree, meaning that in the intensity interval of the control pulse in the present aperture scan, this sign of gradient is the correct assumption for most intensities.

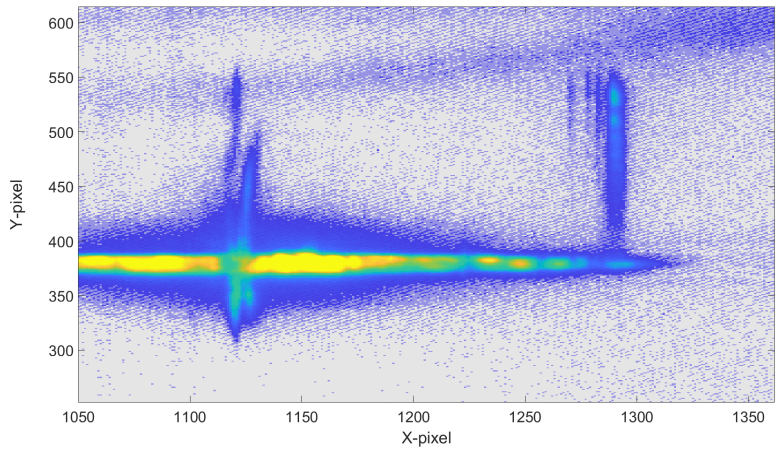


**Figure 4.7:** Detector image showing the difference in behaviour for the $1s2p$-ground state transition line (left-most lines in the figure) compared to the spectral lines of transitions from the higher energy states to the ground state (right side of the spectrum, separated from the on-axis light). This difference can be explained by different Stark shifts from an IR pulse.

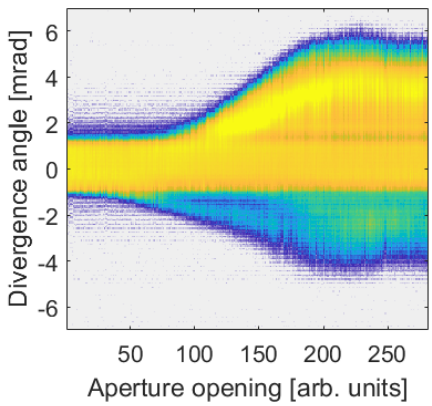


**Figure 4.8:** The measured XUV intensity distribution at the detector, integrated over the frequency region corresponding to a resonant transition between the ground state and $1s2p$ in Helium, shown for each vertical divergence angle as a function of aperture opening. Data corresponding to that presented in [21].

# Chapter 5

# Other Spectroscopy Methods

This chapter describes other spectroscopy methods that I worked with to a lesser extent, and are published in [22] and [23]. These experiments were large collaborations and I have chosen not to include these papers in the thesis as I only have insight of a limited part of the research. However, I still wanted to highlight these in this chapter as they hint at the variety of spectroscopy methods that exist.

The spectroscopy method used in [22] is XUV light from the free electron laser FERMI [24], investigating nitrogen gas injected by a jet in the beamline with a velocity map imaging(VMI) photoelectron spectrometer detection system. The light source in [23] is the same nonlinear high-order harmonic generation process as for the OOM experiments, and the detector is a 3D photoelectron/ion momentum spectrometer.

## 5.1 Experimental investigation at FERMI

Free electron lasers, like FERMI, use the radiation that is emitted from an electron when it is accelerated. This means that the classical description of Sec. 2.1, where the emission is due to the acceleration of the motion of the electron around the nucleus, is relevant also for free electron laser light. By using varying magnetic fields in an undulator, it is possible to single out one wavelength that will be constructively amplified along the beampath, when others will be washed out due to destructive interference [25, 26]. By manipulating the magnetic fields in the undulators it is possible to tune the wavelength. Free electron lasers offer an advantage over table-top XUV light sources in their brightness, and their pulse duration is significantly shorter than that available at synchrotrons. However, table-top XUV light sources still offer shorter pulses[26].

In the experiment of [22], a 81 nm pump pulse and a 795 nm probe pulse were used to ionize molecular nitrogen. The variable time delay between the pump pulse and the probe pulse allowed for a time-resolved measurement of the ionization dynamics. A jet was used to inject the gas-phase nitrogen, which had the advantage of cooling the gas as the pressure dropped rapidly upon entrance in the system from the high-pressure environment before the valve in the jet [22]. The photoelectrons were then detected by the VMI: the electrons are collected in cone-shaped electrodes, made to travel through a flight tube and are finally detected by an MCP detection system similar to that of the OOM experiments. By choosing the bias over the electrodes, it is possible to reach velocity-imaging, so that all photoelectrons of the same velocity reach the same point on the detection plane no matter where they start out from [27].

The objective of this particular experiment was to study the dynamics of Rydberg states of the high-energy part of molecular nitrogen, where the setup described above could improve previously published work. The improvements were possible through the evaluation of the angular distribution of the photoelectron velocities, and the cooling of the nitrogen gas which allowed for longer coherence times and therefore enabled reliable measurements at longer time delays [22].

## 5.2 Coincidence experiments with extreme ultraviolet light and a 3D photoelectron/ion momentum imaging spectrometer

The light source and optical setup that is used in the setup presented in [23] is rather similar to that of the OOM experiments, with a few exceptions. The main difference lies in the higher repetition rate and that it has a 3D photoelectron/ion momentum imaging spectrometer instead of the reflection grating of the OOM setup. The higher repetition rate results in a lower peak power per pulse, which requires a tighter focusing and higher gas pressure for the high-order harmonic generation process. This in turn requires an advanced vacuum system with a catcher pump very close to the gas inlet, to prevent re-absorption, in addition to a turbo pump keeping the ambient chamber pressure low [23].

The 3D photoelectron/ion momentum imaging spectrometer uses an applied electrical field to accelerate photoelectrons toward one detector, and ions to another detector on the opposite end of the vacuum chamber. An applied magnetic field is used to make sure the electrons travel in helical paths where the radius of the helical motion provides information on their momentum [23]. The detectors both consist of MCPs and anode delay lines, so that the timing of when a charged particle hits the detector is handled by the MCPs, and the position is determined by the layers of crossed delay lines [28]. For the electrons, there are three layers of delay lines with a 60° angle between each

layer of delay lines. The added third layer provides enough extra information that multiple electrons can be detected and position-determined simultaneously, which enables coincidence studies.

The setup was used to study double-ionization of Helium with an attosecond pulse train, where the simultaneous detection of two electrons and one ion was used to find the angular distribution of the correlated electrons making up a two-electron wave packet. However, due to a low detection rate time-resolved pump-probe studies of this phenomenon was not possible with the setup at the time of writing.

# Chapter 6

# Outlook

This chapter focuses solely on the outlook for the OOM technique. There are several different directions that the technique could evolve in and be used in different ways. For the setup used for Paper I and Paper II, some changes were made after the data in Paper I and Paper II were collected.

One change is that an SLM was installed on a piezo-stage in the probe arm of the interferometer. This should introduce multiple advantages: previously, there was a risk of changing the focus when the delay was changed, as the mirror on the stage that introduced the delay is not flat. If the focus position changes, the interaction region in the gas moves and the gas density is likely to change. The addition of an SLM to the setup is also a significant possibility for new experiments and improvements. The consequence of these changes will be discussed in more detail in the following sections.

During my last time in the laboratory with the setup, I installed an additional beam-pointing stabilization system. The idea behind installing this system is similar to why it was not optimal to move the focusing mirror when changing the delay; any changes to the focusing risk changing the conditions for the light-matter interaction in the target gas and thus changing parameters that are assumed constant during scans. An improved beam-pointing stabilization helps minimize these issues. The improvement should also help stabilize the focus position of the IR pump pulse in the XUV generation gas, which should improve the stability of the properties of the XUV pulse (see for example [29] for how changes in gas density can affect the resulting XUV beam).

## 6.1 Controlling extreme ultraviolet light with opto-optical modulation

The addition of an SLM to the setup significantly enhances the shaping possibilities. In the papers discussed in this thesis, the shaping possibilities were restricted to a bell-shaped control pulse. An example of the possibilities of extended control pulse shapes can be seen in Fig. 3.5c: if a quadratic shape of the control pulse in the interaction region can be obtained, controlling the focusing of the XUV pulse should be possible. Another example is that of a triangular control pulse shape in the focus: this should enable a variable XUV-beamsplitter, where the intensity in each arm should be possible to regulate by changing the relative center positions of the control pulse and the XUV pulse. If the control pulse is divided into two pulses, these could be made to interfere in the focus, and an optically-induced XUV transmission grating effect could be possible.

These speculations are only a small fraction of the different shaping possibilities that an SLM opens up for, and I am excited to see what results can be produced from this. In a larger perspective, it would be interesting to see whether XUV-XUV pump-probe experiment would be more easily performed by utilizing OOM to steer the pulses. As of today, my impression is that such experiments are rare as they are difficult to perform, and perhaps an improved OOM technique could facilitate the present restrictions.

## 6.2 Probing the Stark effect with opto-optical modulation

One specific possibility that the addition of an SLM in the setup opens up for is that of creating a more linear control pulse intensity gradient in the focus. In the previous experiments in Paper II, the control pulse intensity had a bell-shaped profile, thus the linearity of the control pulse intensity gradient over the atomic ensemble was an approximation. This means that if for example the experiment in Paper II was repeated with an SLM controlling the intensity profile of the control pulse, a more linear intensity gradient across the atomic ensemble could be set up. Then, it could be trusted that any non-linearity is caused by non-linearities in the relation between the Stark shift and the control pulse intensity. As of writing, this ideal situation is not yet obtained. This can be seen for example when comparing Fig. 4.4a and Fig. 4.8: the overall shape of how the emission in Fig. 4.8 moves further and further away from the on-axis light is similar to that of Fig. 4.4a. For this example, my interpretation is that the curvature of how the position of the maximally re-directed emission changes with aperture opening is due to the bell-shape of the control pulse intensity, as the

curvature is similar to that of Fig. 4.4a. For Fig. 4.4a, the states studied are high enough in energy that the Stark shift should depend linearly on the external field intensity and therefore any impact of Stark effect non-linearity with intensity should be small. Thus, the effect of shaping can be seen also when the objective is to study the Stark effect behaviour with control pulse intensity - where it would be ideal to not have any shaping effects due to the intensity profile of the control pulse.

## 6.3 Other spectroscopic measurements with opto-optical modulation

There is one aspect of using OOM to do spectroscopic measurements that I have not discussed. That is the increase in the signal-to-noise that is possible when the emission from the decaying atoms in the ensemble is spatially separated from the XUV pulse that was used to excite them. This, combined with the pump-probe design of the setup that enables high temporal resolution, should enable high quality lifetime measurements of the atomic states involved in the OOM process. This was attempted in a previous experiment (incidentally for my master's thesis project), but the reproducibility of the measurements was far too low to trust the data. This was speculated to be partially because of focus position fluctuations, and thus it might be possible to get reliable data with the aforementioned additional beam-pointing stabilization system [30].

# References


[1] G. Grynberg, A. Aspect, and C. Fabre, *Introduction to quantum optics: from the semi-classical approach to quantized light.* Cambridge University Press, 2010.

[2] R. P. Feynman, R. B. Leighton, and M. L. Sands, *The Feynman lectures on physics.* Addison-Wesley, 1977.

[3] C. J. Foot, *Atomic physics.* Oxford master series in physics: 7, Oxford University Press, 2005.

[4] J. Stark, "Observation of the separation of spectral lines by an electric field," *Nature*, vol. 92, p. 401, 1913.

[5] P. H. Bucksbaum, R. R. Freeman, M. Bashkansky, and T. J. McIlrath, "Role of the ponderomotive potential in above-threshold ionization," *J. Opt. Soc. Am. B*, vol. 4, no. 5, pp. 760–764, 1987.

[6] C. D. Lin, H. Wei, A. T. Le, and C. Jin, *Attosecond and strong-field physics: principles and applications.* Cambridge University Press, 2018.

[7] S. Bengtsson, E. W. Larsen, D. Kroon, S. Camp, M. Miranda, C. L. Arnold, A. L'Huillier, K. J. Schafer, M. B. Gaarde, L. Rippe, and J. Mauritsson, "Space–time control of free induction decay in the extreme ultraviolet," *Nature Photonics*, vol. 11, no. 4, pp. 252–258, 2017.

[8] J. W. Goodman, *Introduction to Fourier optics.* McGraw-Hill physical and quantum electronics series, McGraw-Hill, 1968.

[9] B. E. A. Saleh and M. C. Teich, *Fundamentals of photonics.* Wiley series in pure and applied optics, Wiley, 2007.

[10] S. Bengtsson and J. Mauritsson, "Ultrafast control and opto-optical modulation of extreme ultraviolet light," *J. Phys. B.*, vol. 52, no. 6, p. 063002, 2019.

[11] D. Strickland and G. Mourou, "Compression of amplified chirped optical pulses," *Optics Communications*, vol. 55, no. 6, pp. 447–449, 1985.

[12] A. McPherson, G. Gibson, H. Jara, U. Johann, T. S. Luk, I. A. McIntyre, K. Boyer, and C. K. Rhodes, "Studies of multiphoton production of vacuum-ultraviolet radiation in the rare gases," *Journal of the Optical Society of America B*, vol. 4, pp. 595–601, 1987.

[13] M. Ferray, A. L'Huillier, X. Li, L. Lompre, G. Mainfray, and C. Manus, "Multiple-harmonic conversion of 1064 nm radiation in rare gases," *J. Phys. B*, vol. **21**, pp. L31–L35, 1988.

[14] K. J. Schafer, B. Yang, L. F. DiMauro, and K. C. Kulander, "Above threshold ionization beyond the high harmonic cutoff," *Phys. Rev. Lett.*, vol. 70, pp. 1599–1602, 1993.

[15] P. B. Corkum, "Plasma perspective on strong field multiphoton ionization," *Phys. Rev. Lett.*, vol. 71, pp. 1994–1997, 1993.

[16] M. Lewenstein, P. Balcou, M. Y. Ivanov, A. L'Huillier, and P. B. Corkum, "Theory of high-harmonic generation by low-frequency laser fields," *Phys. Rev. A*, vol. 49, pp. 2117–2132, 1994.

[17] A. L'Huillier and P. Balcou, "High-order harmonic generation in rare gases with an intense short-pulse laser," *Phys. Rev. Lett.*, vol. 70, p. 774, 1993.

[18] J. Ladislas Wiza, "Microchannel plate detectors," *Nuclear Instruments and Methods*, vol. 162, no. 1, pp. 587–601, 1979.

[19] H. J. Shin, D. G. Lee, Y. H. Cha, K. H. Hong, and C. H. Nam, "Generation of nonadiabatic blueshift of high harmonics in an intense femtosecond laser field," *Phys. Rev. Lett.*, vol. 83, pp. 2544–2547, 1999.

[20] M. B. Gaarde, C. Buth, J. L. Tate, and K. J. Schafer, "Transient absorption and reshaping of ultrafast XUV light by laser-dressed helium," *Phys. Rev. A*, vol. 83, p. 013419, 2011.

[21] E. R. Simpson, M. Labeye, S. Camp, N. Ibrakovic, S. Bengtsson, A. Olofsson, K. J. Schafer, M. B. Gaarde, and J. Mauritsson, "Probing Stark-induced nonlinear phase variation with opto-optical modulation," *Phys. Rev. A*, vol. 100, p. 023403, 2019.

[22] M. Fushitani, S. T. Pratt, D. You, S. Saito, Y. Luo, K. Ueda, H. Fujise, A. Hishikawa, H. Ibrahim, F. Légaré, P. Johnsson, J. Peschel, E. R. Simpson, A. Olofsson, J. Mauritsson, P. A. Carpeggiani, P. K. Maroju, M. Moioli,

D. Ertel, R. Shah, G. Sansone, T. Csizmadia, M. Dumergue, N. G. Harshitha, S. Kühn, C. Callegari, O. Plekan, M. Di Fraia, M. B. Danailov, A. Demidovich, L. Giannessi, L. Raimondi, M. Zangrando, G. De Ninno, P. R. Ribič, and K. C. Prince, "Time-resolved photoelectron imaging of complex resonances in molecular nitrogen," *The Journal of Chemical Physics*, vol. 154, no. 14, p. 144305, 2021.

[23] S. Mikaelsson, J. Vogelsang, C. Guo, I. Sytcevich, A.-L. Viotti, F. Langer, Y.-C. Cheng, S. Nandi, W. Jin, A. Olofsson, R. Weissenbilder, J. Mauritsson, A. L'Huillier, M. Gisselbrecht, and C. L. Arnold, "A high-repetition rate attosecond light source for time-resolved coincidence spectroscopy," *Nanophotonics*, vol. 10, no. 1, pp. 117–128, 2021.

[24] E. Allaria, L. Badano, S. Bassanese, F. Capotondi, D. Castronovo, P. Cinquegrana, M. B. Danailov, G. D'Auria, A. Demidovich, R. De Monte, G. De Ninno, S. Di Mitri, B. Diviacco, W. M. Fawley, M. Ferianis, E. Ferrari, G. Gaio, D. Gauthier, L. Giannessi, F. Iazzourene, G. Kurdi, N. Mahne, I. Nikolov, F. Parmigiani, G. Penco, L. Raimondi, P. Rebernik, F. Rossi, E. Roussel, C. Scafuri, C. Serpico, P. Sigalotti, C. Spezzani, M. Svandrlik, C. Svetina, M. Trovó, M. Veronese, D. Zangrando, and M. Zangrando, "The FERMI free-electron lasers," *Journal of Synchrotron Radiation*, vol. 22, no. 3, pp. 485–491, 2015.

[25] J. M. J. Madey, "Stimulated Emission of Bremsstrahlung in a Periodic Magnetic Field," *Journal of Applied Physics*, vol. 42, no. 5, pp. 1906–1913, 1971.

[26] H. Wiedemann, *Synchrotron Radiation Physics*. Springer International Publishing, 2020.

[27] A. Eppink and D. Parker, "Velocity map imaging of ions and electrons using electrostatic lenses: application in photoelectron and photofragment ion imaging of molecular oxygen.," *Review of Scientific Instruments*, vol. 68, no. 9, pp. 3477 – 3484, 1997.

[28] O. Jagutzki, A. Cerezo, A. Czasch, R. Dorner, M. Hattas, M. Huang, V. Mergel, U. Spillmann, K. Ullmann-Pfleger, T. Weber, H. Schmidt-Bocking, and G. Smith, "Multiple hit readout of a microchannel plate detector with a three-layer delay-line anode," *IEEE Transactions on Nuclear Science*, vol. 49, no. 5, pp. 2477–2483, 2002.

[29] L. Quintard, V. Strelkov, J. Vabek, O. Hort, A. Dubrouil, D. Descamps, F. Burgy, C. Péjot, E. Mével, F. Catoire, and E. Constant, "Optics-less focusing of XUV high-order harmonics," *Science Advances*, vol. 5, no. 4, 2019.

[30] A. Olofsson, "Possibilities and challenges in temporal control of XUV pulses by opto-optical modulation," 2018. Student Paper.

# Scientific publications

## Author contributions

### Paper I: Spatial control of extreme ultraviolet light with opto-optical phase modulation

I participated in developing the theory and wrote the simulation software. I wrote the manuscript with support and input from the co-authors.

### Paper II: Probing Stark-induced nonlinear phase variation with opto-optical modulation

I participated in developing the theory and writing simulation software. I gave input on the writing of the manuscript.

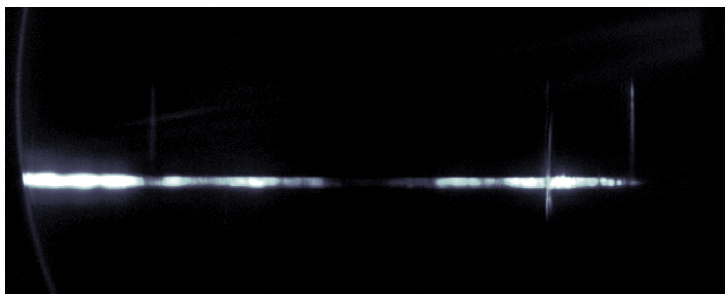

Printed by Media-Tryck, Lund 2021 NORDIC SWAN ECOLABEL 3041 0903

LUND UNIVERSITY
Faculty of Engineering, LTH
Department of Physics
Divison of Atomic Physics

9789178959549 (print)
9789178959532 (pdf )
ISSN: 0281-2762
Lund Reports on Atomic Physics, LRAP572 (2021)